Generalized Model of Modular Two Element Compensated IPT Systems with Common DC-Bus

Enes Ayaz, Ogün Altun, Hakan Polat, Ozan Keysan

In this paper, modular IPT systems which have receiver series/parallel compensation with series/parallel common DC-Bus are investigated. For these systems, power sharing between the receiver modules is vulnerable to system components such as the mutual coupling between the transmitter and the receiver coils. It is also observed that the power sharing is affected by the compensation topologies of the receivers and the type of the electrical connection of common DC-Bus. Therefore, in this study, a mathematical model is presented to reveal the power sharing characteristics in terms of operating frequency and mutual inductance differences of the modules. Then the mathematical model is verified for series compensated, series/parallel connected IPT systems with single transmitter-two receivers, and 5% mean error is achieved.

***Index Terms*—Wireless power transfer, inductive power transfer, modular design, multiple receiver, common DC Bus**

List of Abbreviations

ω	Operation angular frequency
ω_0	Resonant angular frequency
C_{RX}	Compensation capacitor capacitance of the Rx module
$I_{RX(i)}$	AC current flowing across the i^{th} Rx module
L_{RX}	IPT coil inductance of the Rx module
$M_{(i)}$	Mutual inductance between the Tx and i^{th} Rx module IPT coils
P	Output power on the load
P_i	Power of the i^{th} Rx module
Q_{RX}	Quality factor of the Rx module
$R_{RX(i)}$	Equivalent resistance seen by the inputs of the diode rectifier of i^{th} Rx module
R_{RX}	Equivalent resistance seen by the inputs of diode rectifier
$V_{RX(i)}$	AC voltage across at the input of the diode rectifier of the i^{th} Rx module
$V_{RX(i)}$	Induced voltage on the i^{th} Rx module IPT coil
V_{TX}	AC current flowing across the Tx side IPT coil
Z_{RX}	The impedance of the resonant tank of the Rx module
n	Number of Rx modules

I. Introduction

Inductive power transfer (IPT) systems have gained popularity due to developments in semiconductor technologies and an increase in the computational power of micro-controllers. Spatial freedom and cordless design make IPT systems highly consumer-friendly. Moreover, galvanic isolation in IPT systems increases the safety. It has many applications with different power levels ranging from phone chargers [1], and biomedical implants [2] to ultra-fast EV chargers [3].

Most conventional IPT systems have DC to AC stage where high-frequency AC current flows from the transmitter (Tx) coil. This varying AC magnetic flux is coupled by the receiver (Rx) coil. Then, the induced voltage is rectified, often employing diode rectifiers. Similar to isolated power converter topologies, the Tx and Rx coils form a magnetic coupling. However, for IPT systems, the windings are loosely coupled making the power factors highly inductive. In order to obtain unity power factor, both Tx and Rx sides should be compensated using either series or parallel connected capacitors. There are four common compensation topologies used in IPT systems named according to the type of connection: series-series (SS), series-parallel (SP), parallel-parallel (PP), parallel-series (PS) [4]. Primary series connection is used with voltage source inputs, whereas the primary parallel connection requires current source input. Similarly, secondary series compensation acts as a voltage source on the output, and secondary parallel compensation provides current source behavior on the output side.

The power rating of an IPT system is determined by the topology and the semiconductor ratings. Series compensation is problematic due to capacitor sizing and voltage rating due to high-frequency AC current [5]. Moreover, as the power rating increases, the operation frequencies usually reduce, which also increases the size of the system. In order to reduce the system size and cost, modular IPT systems are proposed to reduce power ratings of each semiconductor, increase modularity and simplify thermal management. Another advantage of modular systems is selective power transmission where the frequency is varied to control the ratio of power transfer between two different loads [6]. Another advantage of modular Rx coils connected to a common DC-bus is improved misalignment. Ke *et. al* investigate a multi-coil design with a common DC-bus, and propose receiver parallel compensated parallel DC-bus to mitigate misalignment problems [7]. In [8], LCC-LCC compensation is used with parallel connected Rx modules. Multi Tx modules are used to achieve rotational misalignment tolerance. Another LCC-LCC compensation WPT system is proposed in [9]. Two Tx modules and two Rx modules are used for compactness and the outputs of the Rx modules are connected in parallel to achieve high power output. A 10kW four receiver wireless power transfer system is designed in [10] for dynamic EV charging. Series-series compensation is used in the system and outputs are grouped in pairs, connected in parallel and series which reduces the output fluctuation. In [11], transmitter series, receiver parallel compensation is used with a 7 kW design and the input parallel, output series IPT system is proposed to obtain a high output voltage. In [12], a 6 kW prototype was built using three 2 kW modules,

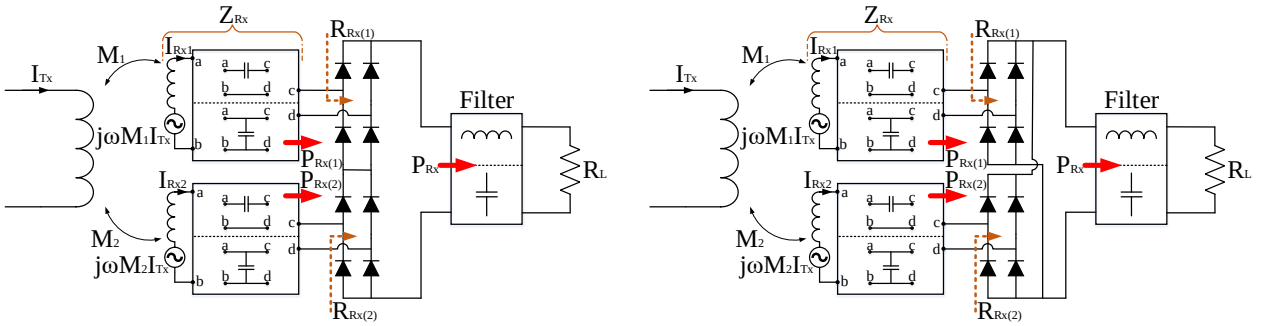

(a) Series connected common DC-Bus.

(b) Parallel connected common DC-Bus.

Fig. 1. Series and parallel connected common DC-Bus

where LCL-T topology is used. The outputs are connected in parallel to achieve redundancy and to increase fault tolerance. A WPT system based on dual transmitters and dual receivers presented in [13] aims to increase the power transfer capability with four transmission paths. Modular design provides lower cost and lower semiconductor ratings and improves the system reliability. Another application combining these two advantages is contactless slip-ring design presented in [14]. 2Tx-4Rx IPT coils are placed around a rotating shaft. The system is series-series compensated, and the outputs of the Rx modules are connected in parallel to a common DC-bus. In [15], a series-series compensated, common DC-bus is used with a middle-stage resonator, to improve the fault tolerance. Although there are many studies about IPT systems with common DC-bus, power-sharing problem of these systems are not much investigated in generalized manner.

In this paper, common DC-bus systems with series or parallel compensated Rx side modules will be investigated. Firstly, the power-sharing problem will be discussed for series/parallel load-connected common DC-bus systems. Then a generalized analytical model on common DC-bus will be presented. The analytical model, simulations, and experimental results will then be compared.

II. Common DC-Bus- Compensation Topologies

The output of the Rx modules can be connected either in series or parallel to form a common DC-Bus on the output side, as presented in Fig. 1. Parallel connected modules, as shown in Fig. 1-a, have the same DC output voltage, and the output current is shared by the modules. This way, less current flows through each Rx module, and the current rating of the semiconductor devices is reduced compared to a single Rx configuration. For series-connected modules as in Fig. 1-b, DC-Bus voltage is the sum of module output voltages, while the current of each module is the same. Series connection of the modules allows higher voltage levels at the output. Semiconductor voltage ratings are reduced compared to a single Rx system.

In the case of equal magnetic coupling between Tx and each Rx modules, voltage is shared equally for series-connected modules, and current is divided equally for parallel-connected modules. However, when the couplings between Tx and each Rx module are not equal, voltage is not shared equally for series modules, and the current unbalance occurs for parallel modules. Thus, uneven power distribution occurs between Rx modules. Unbalanced power distribution increases the semiconductor stresses and overall system losses which worsens the thermal management.

III. Mathematical Modelling of Common DC-Bus

In a multi-Rx system with a common DC-Bus, uneven power distribution stems from unequal reflected module resistances. In (1), the reflected resistances of a single-Rx system, having Rx side series and parallel compensation, are given. This formulation is derived assuming that the system operates at continuous conduction mode (CCM) [16], [17] and the first harmonic approximation (FHA) is valid.

$$R_{RX} = \begin{cases} \dfrac{8}{\pi^2} R_L & \text{series compensation} \\ \dfrac{\pi^2}{8} R_L & \text{parallel compensation} \end{cases} \tag{1}$$

For the multi-Rx system, if the mutual inductance, resonant circuit elements, and parasitic components of each module are equal to the other, the reflected resistances are distributed as in (2) for the series and parallel load connection.

$$R_{RX(i)} = \begin{cases} \dfrac{R_{RX}}{n} & \text{series modules} \\ nR_{RX} & \text{parallel modules} \end{cases} \tag{2}$$

However, if the circuit parameters of Rx coils, such as mutual inductance, quality factor, etc., are different, the reflected resistances of modules can differ, which results in the uneven power distribution problem. In this section, the change on the reflected resistances is analytically modeled. Calculations are made considering a system with two modules for ease of analytical derivation, but it can be generalized to a system with N-modules. The IPT coil inductances and compensation capacitances of the modules are assumed to be equal.

Firstly, the induced voltages of Rx coils are calculated as in (3). The induced voltages of Rx coils depend on the mutual inductances, but for the Tx side, the only I_{TX} is used in the following calculations.

$$V_{RX(i)} = j\omega M_{(i)} I_{TX} \tag{3}$$

According to the electrical connection of Rx's, the current or voltage magnitudes of modules are equal. Therefore, the current of each module is the same for series-connected modules, as given in (4), and the voltage of each module is the same for parallel-connected modules as presented in (5). At this point, calculations are presented in four sections, considering the series/parallel compensation with the series/parallel load connection of the modules.

$$|I_{RX(1)}| = |I_{RX(2)}| \tag{4}$$

$$|V_{RX(1)}| = |V_{RX(2)}| \tag{5}$$

A. Receiver Series (RS) Compensation with Series Modules (SM) Connection

The frequency-domain lumped circuit of RS-SM is shown in Fig. 2. By assuming that both modules operate simultaneously, the modules' currents, which are also the currents of receiver coils, are equal to each other, as shown in (6). The Z_{RX} is receiver impedance, defined in (7).

$$I_{RX(1)} = I_{RX(2)} = \frac{j\omega(M_{(1)} + M_{(2)})I_{TX}}{2Z_{RX} + R_{RX}} \tag{6}$$

$$Z_{RX} = j\omega L_{RX} + \frac{1}{j\omega C_{RX}} \tag{7}$$

The reflected resistance for each module is calculated using

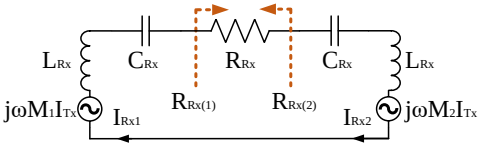

Fig. 2. The lumped circuit of series connected modules with receiver series compensation.

(8). It is observed that the reflected resistances are distributed proportional to the mutual inductance of the modules. Moreover, the power ratio of modules is also proportional to the reflected resistance as the modules share current equally. Therefore, the power distribution of the first module is obtained analytically in (9) and plotted in Fig. 3.

$$\begin{aligned} R_{RX(1)(2)} &= \Re\left(\frac{j\omega(M_{(1)(2)})I_{TX}}{I_{RX(1)(2)}}\right) \\ &= R_{RX}\frac{M_{(1)(2)}}{M_{(1)} + M_{(2)}} \end{aligned} \tag{8}$$

$$\begin{aligned} \frac{P_{(1)}}{P_{(1)} + P_{(2)}} &= \frac{I_{RX(1)}^2 R_{RX(1)}}{I_{RX(1)}^2 R_{RX(1)} + I_{RX(2)}^2 R_{RX(2)}} \\ &= \frac{M_{(1)}}{M_{(1)} + M_{(2)}} \end{aligned} \tag{9}$$

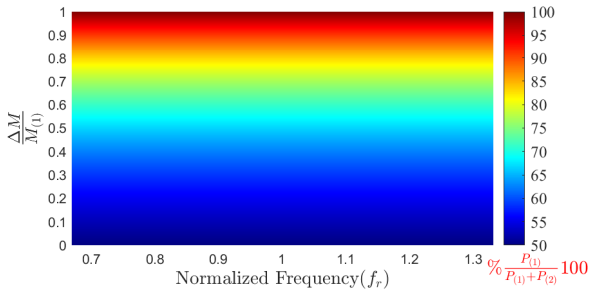

Fig. 3. The power distribution of one module for series compensated series modules in terms of different frequencies and mutual differences.

Although the uneven power distribution stems from the mutual inductance difference, it is also influenced by the operating frequency. Therefore, the power distribution should be given in terms of both mutual inductance difference and operating frequency. For Fig. 3, the horizontal axis shows the operating frequency normalized by resonant frequency, and the vertical axis shows the normalized mutual inductance difference. The colormap shows the power ratio of one module to the total power. Thus, while 100 percent means that only one module transfers power, 50 percent shows that the modules share the power equally.

B. Receiver Series (RS) Compensation with Parallel Modules (PM) Connection

In Fig. 4, the lumped circuit of RS-PM is presented. For parallel-connected modules, the sum of the reflected conductance of modules gives the complete reflected conductance, as given in (10).

$$\frac{1}{R_{RX(1)}} + \frac{1}{R_{RX(2)}} = \frac{1}{R_{RX}} \tag{10}$$

The module's voltages are equal for the system, and they are calculated as in (6). The Z_{RX} is the same as SC-SM, as given in (7).

$$V_{RX(1)(2)} = R_{RX(1)(2)}\frac{j\omega M_{(1)(2)} I_{TX}}{Z_{RX} + R_{RX(1)(2)}} \tag{11}$$

Then, the equality condition of the module's voltages is

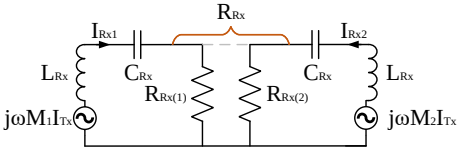

Fig. 4. The lumped circuit of parallel connected modules with receiver series compensation.

obtained as in (12), and it is brought into a closed form, as given in (13) where α is defined as $\frac{M_{(1)}}{M_{(2)}}$.

$$|R_{RX(1)}\frac{M_1}{Z_{RX} + R_{RX(1)}}| = |R_{RX(2)}\frac{M_2}{Z_{RX} + R_{RX(2)}}| \tag{12}$$

$$0 = ((\alpha^2-1)R_L^2 - |Z_S|^2)R_1^2 + 2R_LR_1 + (\alpha^2-1)|ZsR_L|^2 \tag{13}$$

The quadratic equation in (13) can be solved, and the reflected resistance of the first module can be calculated as in (14). The ratio of modules' power is presented in general form as a function of the quality factor of the load Q_{RX}, defined as $\frac{\omega_o L_{RX}}{R_{RX}}$, presented in (15).

$$R_{RX(1)} = \frac{R_{RX}|Z_{RX}|^2}{(1-\alpha^2)R_{RX}^2 + |Z_{RX}|^2} + R_{RX}Z_{RX}\frac{\sqrt{|Z_{RX}|^2\alpha^2 - R_{RX}^2(1-\alpha^2)^2}}{(1-\alpha^2)R_{RX}^2 + |Z_{RX}|^2} \tag{14}$$

$$\frac{P_1}{P} = \frac{R_{RX}}{R_{RX(1)}} = \frac{(1-\alpha^2)\frac{\omega^2\omega_o^2}{Q_{RX}(\omega^2-\omega_o^2)} + 1}{1 + \sqrt{\alpha^2 + ((1-\alpha^2)^2\frac{\omega^2\omega_o^2}{Q_{RX}(\omega^2-\omega_o^2)})}} \tag{15}$$

The power distribution of one module is plotted in Fig. 5, as a function of frequency and the normalized mutual inductance difference between the modules. The power distribution at the resonant frequency is susceptible, and the power is transferred by only one module if a slight change in mutual inductance. However, the power distribution becomes better as the operation frequency is farther away from the resonant frequency.

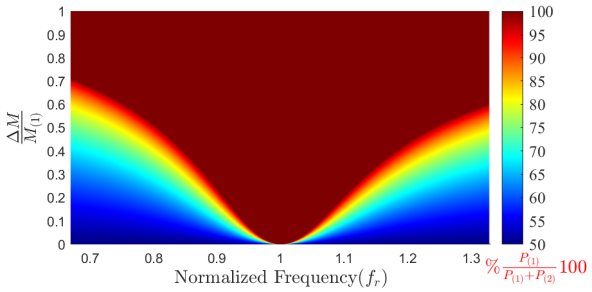

Fig. 5. The power distribution of one module for series compensated parallel modules in terms of different frequencies and mutual differences.

C. Receiver Parallel (RP) Compensation with Parallel Modules (PM) Connection

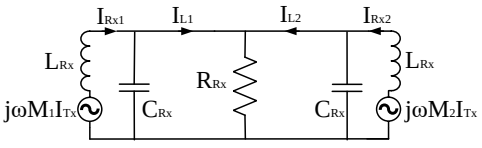

Fig. 6. The lumped circuit of parallel connected modules with receiver series compensation.

The lumped circuit of RP-PM is shown in Fig. 6. Unlike the series compensation, the module current and Rx current are not equal for each module. A mesh equation is established to solve the circuit and calculate the reflected resistance of each module. The Z, I, and V matrices are given in (16), (17), and (18) respectively.

$$Z = \begin{bmatrix} Z_{RX} & \frac{-1}{j\omega C_{RX}} & 0 & 0 \\ \frac{-1}{j\omega C_{RX}} & \frac{1}{j\omega C_{RX}} + R_{RX} & R_{RX} & 0 \\ 0 & R_{RX} & \frac{1}{j\omega C_{RX}} + R_{RX} & \frac{-1}{j\omega C_{RX}} \\ 0 & 0 & \frac{-1}{j\omega C_{RX}} & Z_{RX} \end{bmatrix} \tag{16}$$

$$I = \begin{bmatrix} I_{RX(1)} \\ I_{L(1)} \\ I_{L(2)} \\ I_{RX(2)} \end{bmatrix} \tag{17}$$

$$V = \begin{bmatrix} j\omega M_1 I_{TX} \\ 0 \\ 0 \\ j\omega M_2 I_{TX} \end{bmatrix} \tag{18}$$

The module currents can be calculated using (19). Then, the reflected resistance is found by the module current, assuming that the voltages of modules are equal and that the sum of conductances of each module give the total conductance as in (10).

$$I = Z^-1V \tag{19}$$

The reflected resistance is given in (20). Moreover, the power distribution of one module is presented in (21) and shown in Fig. 7. The power distribution changes moderately depending on a mutual difference, and also, the power distribution is better at the operating frequency close to the resonant frequency.

$$R_{RX(1)} = R_{RX}\frac{I_{L(1)} + I_{L(2)}}{I_{L(1)(2)}} \tag{20}$$

$$\frac{P_{(1)}}{P} = \frac{I_{L(1)}}{I_{L(1)+I_{L(2)}}} \tag{21}$$

D. Receiver Parallel (RP) Compensation with Series Modules (SM) Connection

The lumped circuit of RP-PM is shown in Fig. 8. The modules' currents, which differ from the Rx coil currents, are equal.The total reflected resistance is calculated by modules' reflected resistances as presented in (22).

$$R_{RX(1)} + R_{RX(2)} = R_{RX} \tag{22}$$

The module currents can be found by (23), where $Z_{RX}$is the impedance of parallel-connected L_{RX} and C_{RX}, as given in (24).

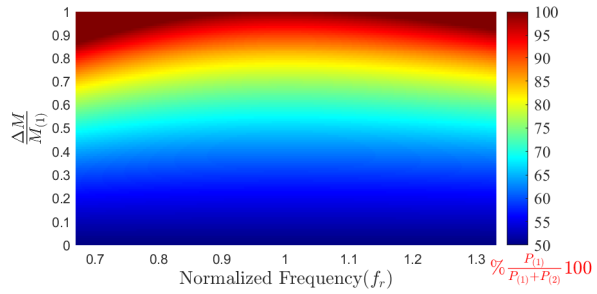

Fig. 7. The power distribution of one module for parallel compensated parallel modules in terms of different frequencies and mutual differences.

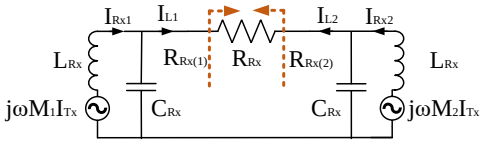

Fig. 8. The lumped circuit of parallel connected modules with receiver series compensation.

$$I_{L(1)(2)} = (1 - \frac{w^2}{w_o^2})\frac{j\omega M_{(1)(2)} I_{TX}}{Z_{RX} + R_{RX(1)(2)}} \tag{23}$$

$$Z_{RX} = \frac{j\omega L_{RX}}{1 - \frac{w^2}{w_o^2}} \tag{24}$$

The equality of modules' currents is obtained in (25), and it can be brought in closed form, as shown in (26). Unlike RS-PM, the β is $\frac{\mathrm{M}_{(1)}^2 - \mathrm{M}_{(2)}^2}{\mathrm{M}_{(1)}^2}$.

$$|(1 - \frac{w^2}{w_o^2})\frac{j\omega M_1 I_{TX}}{Z_{RX} + R_{RX(1)}}| = |(1 - \frac{w^2}{w_o^2})\frac{j\omega M_2 I_{TX}}{Z_{RX} + R_{RX(2)}}| \tag{25}$$

$$\begin{aligned} 0 = {} & \beta R_{RX(1)}^2 - 2R_{RX}R_{RX(1)} \\ & + \beta|Z_{RX}|^2 + R_{RX}^2 \end{aligned} \tag{26}$$

Then, the reflected resistance of the first module is calculated as in (27). Moreover, the ratio of modules' power is brought in the general form as a function of the quality factor of the load $\mathrm{Q_{RX}}$, defined as $\frac{\mathrm{R_{RX}}}{\omega_o \mathrm{L_{RX}}}$, as presented in (28).

$$R_{RX(1)} = \frac{R_{RX} - \sqrt{(1-\beta)R_{RX}^2 - |Z_{RX}\beta|^2}}{\beta} \tag{27}$$

$$\frac{P_1}{P} = \frac{R_{RX(1)}}{R_{RX}} = \frac{1 - \sqrt{(1-\beta) - \frac{\omega^2\omega_o^2}{(\omega_o^2 - \omega^2)^2 Q_{RX}^2}}}{\beta} \tag{28}$$

The power distribution of one module is plotted as a function of frequency and the normalized mutual difference between the modules in Fig. 9. The power distribution at the resonant frequency is susceptible like RS-PM. However, the power distribution becomes better at operation frequency, far from the resonant frequency.

TABLE I
THE SIMULATION AND MATHEMATICAL MODEL PARAMETERS

	RS-SM	RS-PM	RP-PM	RP-SM
$L_{RX}(\mu H)$	18	18	6	6
$C_{RX}(nF)$	62.5	62.5	187.5	187.5
$R_{RX}(\Omega)$	5	20	5	20
$I_{TX}(A)$	2	2	2	2
$M(\mu H)$	4	4	2	2
Q_{RX}	4.2	1.05	1.1	4.4

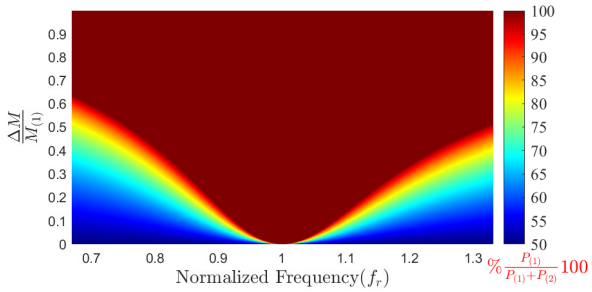

Fig. 9. The power distribution of one module for parallel compensated series modules in terms of different frequencies and mutual differences.

IV. Simulation Results

In this section, a series of simulations are made to verify the mathematical models. In mathematical models, the power distribution depends on the quality factor of receivers, the mutual difference between receivers, and the normalized frequency of receivers. In order to compare each operation point over the range of frequencies and mutual differences, simulation parameters are selected as presented in Table I.

Simulation results as a function of frequency and mutual difference are given in Fig. 10. Both simulation results and mathematical models have good arrangement. However, some deviations for some specific regions are observed. The regions are confined in white lines as shown in Fig. 10. Also, the amount of deviation is given in terms of the error function of (29).

$$\epsilon = \%|\frac{P_{d-sim/exp} - P_{d-mat}}{P_{d-sim/exp}}| \tag{29}$$

The mathematical models are established assuming that CCM operation is maintained and FHA is valid, which means parallel-connected receiver currents have a sinusoidal current shape as well as series-connected receiver voltages are perfect sinusoidal. However, the system operates in DCM for some range of operating frequency and mutual difference due to the non-linearity of rectifier diodes. Hence, FHA is not valid and, the mathematical model deviates from the simulation results due to DCM operations.

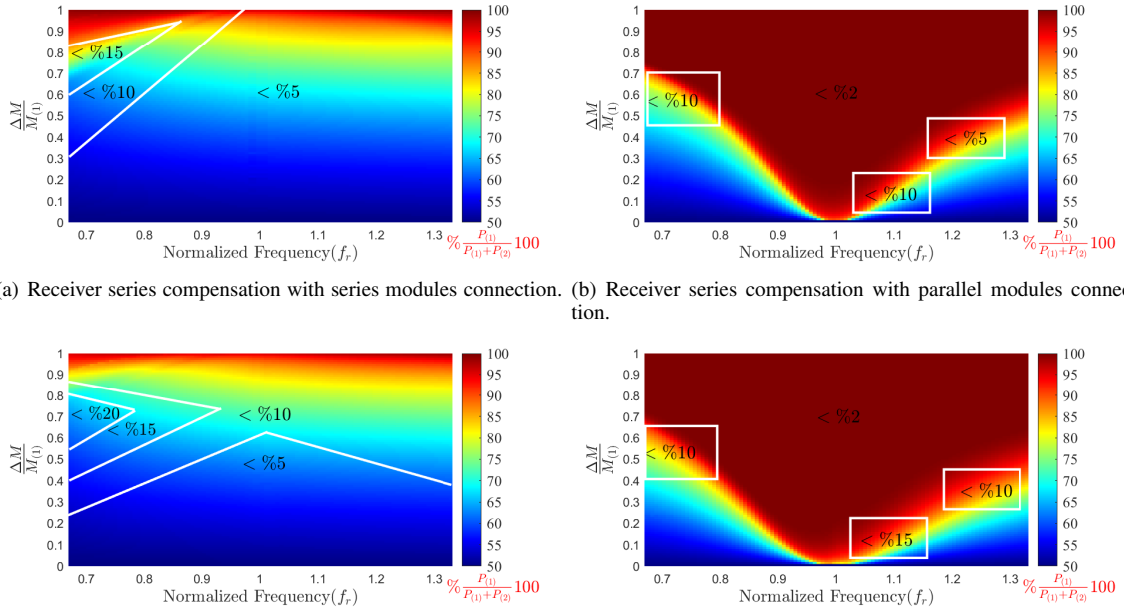

(a) Receiver series compensation with series modules connection.

(b) Receiver series compensation with parallel modules connection.

(c) Receiver parallel compensation with parallel modules connection.

(d) Receiver parallel compensation with series modules connection.

Fig. 10. The power distribution of one module for different frequency and mutual difference: The percentages on the figures show the errors between mathematical model and simulation results. Values are independent of the power distribution percentage and calculated according to (29).

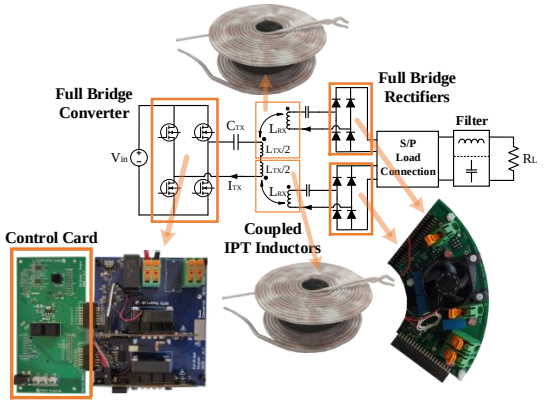

Fig. 11. Experimental setup for RS-SM/PM system.

TABLE II
EXPERIMENTAL SETUP PARAMETERS

Rx side Recrifier Diodes	C3D10060G
Litz Wire	400x0.08mm (2 mm^2)
Tx coil D_{in} and D_{out} (mm)	10-62
Tx coil # of turns	13 each
Rx coil D_{in} and D_{out}	10-74
Rx coil # of turns	16 each
C_{Tx} (nF)	47.5
C_{Rx} (nF)	62.5
Airgap (mm)	20
f_0	150 kHz
Ferrite shield	I20x2 N48 (70x80mm total)

V. EXPERIMENTAL RESULTS

Although a high agreement was observed with the analytical model and simulation results, an experimental verification is still necessary. From Fig. 10, the power distribution characteristics of RS-PM and RP-SM is similar. The same is also true for RS-SM and RP-PM. Therefore, the experimental verification is only performed for RS-SM/PM. The experimental setup is presented in Fig. 11. To be able to adjust the mutual inductance difference, the Tx side coil has two series-connected coils. Each Tx coil is coupled with a single Rx coil, and the distances between the coupled inductors are adjusted such that no cross-coupling is present. The Tx side GaN-based full-bridge converter and Rx side full bridge diode rectifiers are presented in [18] and [19] respectively. The details of the experimental setup are given in Table II.

$$L(\mu H) = \begin{cases} \begin{bmatrix} 22.91 & 3.00 & 3.92 \\ 3.00 & 17.09 & 0 \\ 3.92 & 0 & 17.16 \end{bmatrix} & \Delta M = 0.24 \\ \begin{bmatrix} 22.88 & 4.13 & 2.45 \\ 4.13 & 17.10 & 0 \\ 2.45 & 0 & 17.08 \end{bmatrix} & \Delta M = 0.40 \end{cases} \quad (30)$$

The experimental results are obtained for $\Delta M = 0.24$ and $\Delta M = 0.4$ for RS-SM and RS-PM configurations. The inductance matrix for the mutual differences is presented in (30) where the $\Delta M = 0.24$ and $\Delta M = 0.4$ are presented in color red and blue, respectively. The experimental results are shown for RS-SM in Fig. 12.a, where the results are highly consistent with mathematical model. The results are obtained between 100kHz and 200kHz operating frequencies for the mutual differences of $\Delta M = 0.24$, and $\Delta M = 0.40$. The

mean errors, which are defined as the average of differences between the measured data and mathematical calculations, are found as $\%2.26$ and $\%2.86$ for $\Delta M = 0.24$ and $\Delta M = 0.40$ respectively. In lower operating frequencies (<120kHz) the system enters into DCM for higher ΔM. So, the mathematical model results deviate from the experimental results, as shown in the simulation results. Therefore, the mean error between the mathematical model and experimental results increases by increasing ΔM for RS-SM. Moreover, the experimental results are shown in Fig. 12.b for RS-PM with the same parameters. Results are generally matching with the mathematical model. The mean errors are calculated as $\%4.31$ and $\%3.34$ for $\Delta M = 0.24$ and $\Delta M = 0.40$ respectively. The mathematical model deviates from the experimental results for RS-PM in the inductive region as observed in the simulation results. The frequency, which the deviation begins, increases with mutual inductance difference. Current waveforms of an example of deviated frequency for two mutual inductance differences are shown in Fig. 13 to confirm the DCM operation.

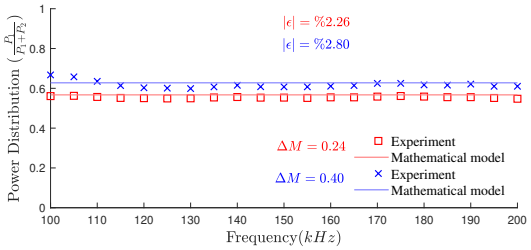

(a) Series modules.

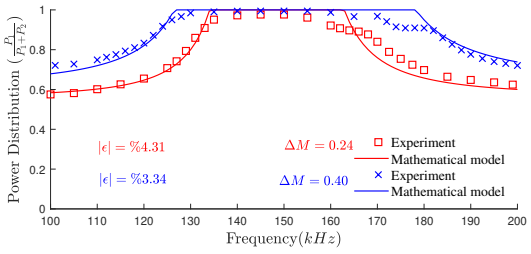

(b) Parallel modules.

Fig. 12. The power distribution of one module for two different ΔM.

VI. Discussion

Until this point, the power-sharing problem for common DC-bus is analytically modeled and verified using simulation and experimental results. At this point, a comparison will be presented with respect to different parameters.

Multi-Rx configurations can be applied to achieve a modular and fault-tolerant system with lower semiconductor stress. However, in section 2, it was shown that the multi-Rx systems do not have these desired advantages due to an uneven power distribution problem. Still, the problem can be mitigated with the proper selection of compensation method and electrical connection type. In this section, the four systems, RS-SM, RS-PM, RP-PM, and RP-SM, are compared in terms of their sensitivity to coupling differences, one-module operation, semiconductor stress, efficiency, output filter type, and resonant capacitor sizing.

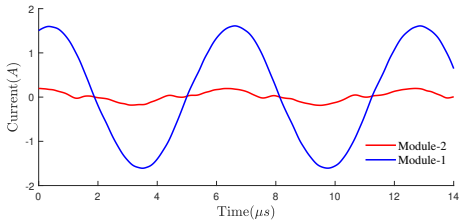

(a) $\Delta M = 0.24$ @160kHz.

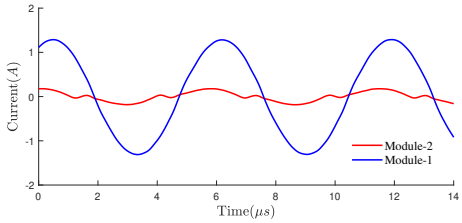

(b) $\Delta M = 0.40$ @170kHz.

Fig. 13. DCM operation of RS-PM. The selected frequencies are taken at high error locations as presented in Fig. 10. (The resonant frequency of the Rx side compensation is 150 kHz.)

Table VI presents the comparison of the four systems. Although the power distribution of RS-SM and RP-PM are less sensitive to the coupling differences, the power distribution of RS-PM and RP-SM are highly affected. Therefore, the RS-PM and RP-SM are unsuitable for dynamic applications, such as eV chargers, consumer electronics, etc., as they are susceptible to coupling differences. On the contrary, RS-PM and RP-SM can operate with a lower sensitivity of coupling difference at a frequency far from the resonance frequency, but the efficiency decreases in this operating condition. The second issue is one-module operation due to a short or open circuit faults of a module. In this situation, the power decreases to a quarter for RS-SM and RP-PM while considering the reflected resistance to the Tx side. Besides, the power reduces to half for RS-PM and RP-SM topologies. Another issue is the semiconductor stress. For the transmitter side, the Tx current and voltages are the same for all systems. However, series-connected receiver modules share the voltage, and parallel-connected receiver modules share the current. Hence, while the stress of Tx side semiconductors remains the same, the stress of the Rxs' side semiconductors decreases. In other aspects of sharing the voltages or currents, the systems' efficiency differs from each other. The majority of the losses stem from the conduction losses of the diodes and the coils' resistance, so the series-connected modules have higher losses than parallel-connected modules. Then, output filter requirements of each system can be argued. For series-compensated systems, a capacitive output filter is suitable not to distort the Rx coil current. However, an inductive filter is more appropriate for parallel-compensated systems not to distort the Rx capacitor voltage. The final concern is the size of the resonant capacitor. The size of the resonant capacitor of the series-compensated system is smaller than the parallel-connected system. Additionally, the resonant capacitor of the series-compensated system decreases if modules are connected series, and the opposite is valid for parallel-compensated systems.

TABLE III
THE COMPARISON OF FOUR SYSTEMS, RS-SM, RS-PM, RP-PM AND RP-SM

Topology / *Paramaters*		**RS-SM**	**RS-PM**	**RP-PM**	**RP-SM**
The sensitivity to coupling differences		Moderate	Bad	Moderate	Bad
One module fault condition		0.25 p.u	0.5 p.u	0.25 p.u	0.5 p.u
Diodes stress	**Voltage**	0.5 p.u	1 p.u	1 p.u	0.5 p.u
	Current	1 p.u	0.5 p.u	0.5 p.u	1 p.u
Efficiency		Moderate	Higher	Moderate	Higher
Output filter type		Capacitive	Capacitive	Inductive	Inductive
Resonant capacitor sizing		Higher	The same	Higher	The same

VII. CONCLUSION

In this paper, multi-Rx systems with common DC-Bus have been investigated. In these systems, uneven power distribution occurs due to mutual inductance differences between the modules. However, it was observed that receivers' compensation types influence the power distribution. Although the effect of compensation type on the power distribution is explained as a voltage or current source with internal impedances, which represent the induced emf from mutual inductance and compensation circuit, there is no generalized mathematical modeling of the power distribution in the literature. In this paper, a generalized mathematical model for receiver series and parallel compensations was proposed. Hence, the compensation method for a multi-Rx common-DC bus can be selected using the mathematical model. On the one hand, the mathematical model has shown us that in systems operating at the resonant frequency, RS-SM and RP-PM are quite insensitive to mutual inductance differences. On the other hand, RS-PM and RP-SM are drastically affected by mutual inductance differences, which can even result to losing modularity and transferring the power with single module. However, if the operating frequency moves away from the resonant frequency, the power distribution of RS-PM and RP-SM gets better. While RS-SM and RP-PM are advantageous in providing well power distribution regardless of the frequency, other systems can also be used considering fault-tolerance, modularity, and efficiency. In order to verify the mathematical model, an experimental setup of RS-SM and RS-PM is established, and experimental results verified the mathematical model with lower than 5% error. Furthermore, the results were also verified RP-PM and RP-SM since they are dual of RS-SM and RS-PM.

REFERENCES

[1] S. Y. R. Hui and W. W. C. Ho, "A new generation of universal contactless battery charging platform for portable consumer electronic equipment," *IEEE Trans. Power Electron.*, vol. 20, no. 3, pp. 620–627, 2005.

[2] O. Knecht, R. Bosshard, and J. W. Kolar, "High-Efficiency Transcutaneous Energy Transfer for Implantable Mechanical Heart Support Systems," *IEEE Trans. Power Electron.*, vol. 30, no. 11, pp. 6221–6236, 2015.

[3] D. Patil, M. K. McDonough, J. M. Miller, B. Fahimi, and P. T. Balsara, "Wireless power transfer for vehicular applications: Overview and challenges," *IEEE Trans. Transport. Electrific.*, vol. 4, no. 1, pp. 3–37, March 2018.

[4] V. Shevchenko, O. Husev, R. Strzelecki, B. Pakhaliuk, N. Poliakov, and N. Strzelecka, "Compensation topologies in ipt systems: Standards, requirements, classification, analysis, comparison and application," *IEEE Access*, vol. 7, pp. 120 559–120 580, 2019.

[5] B. Fahimi, P. T. Balsara, D. Patil, J. M. Miller, and M. K. McDonough, "Wireless Power Transfer for Vehicular Applications: Overview and Challenges," *IEEE Transactions on Transportation Electrification*, vol. 4, no. 1, pp. 3–37, 2017.

[6] Y. Zhang, T. Lu, Z. Zhao, F. He, K. Chen, and L. Yuan, "Selective wireless power transfer to multiple loads using receivers of different resonant frequencies," *IEEE Transactions on Power Electronics*, vol. 30, no. 11, pp. 6001–6005, 2015.

[7] G. Ke, Q. Chen, W. Gao, S.-C. Wong, C. K. Tse, and Z. Zhang, "Research on ipt resonant converters with high misalignment tolerance using multicoil receiver set," *IEEE Transactions on Power Electronics*, vol. 35, no. 4, pp. 3697–3712, 2020.

[8] Z. Yan, B. Song, Y. Zhang, K. Zhang, Z. Mao, and Y. Hu, "A Rotation-Free Wireless Power Transfer System with Stable Output Power and Efficiency for Autonomous Underwater Vehicles," *IEEE Transactions on Power Electronics*, vol. 34, no. 5, pp. 4005–4008, may 2019.

[9] Y. Li, T. Lin, R. Mai, L. Huang, and Z. He, "Compact double-sided decoupled coils-based wpt systems for high-power applications: Analysis, design, and experimental verification," *IEEE Transactions on Transportation Electrification*, vol. 4, no. 1, pp. 64–75, 2018.

[10] S. Cui, Z. Wang, S. Han, C. Zhu, and C. C. Chan, "Analysis and design of multiphase receiver with reduction of output fluctuation for ev dynamic wireless charging system," *IEEE Transactions on Power Electronics*, vol. 34, no. 5, pp. 4112–4124, 2019.

[11] H. Liu, Q. Chen, G. Ke, X. Ren, and S.-C. Wong, "Research of the input-parallel output-series inductive power transfer system," in *2015 IEEE PELS Workshop on Emerging Technologies: Wireless Power (2015 WoW)*, 2015, pp. 1–7.

[12] H. Hao, G. A. Covic, and J. T. Boys, "A parallel topology for inductive power transfer power supplies," *IEEE Transactions on Power Electronics*, vol. 29, no. 3, pp. 1140–1151, 2014.

[13] Y. Li, R. Mai, T. Lin, H. Sun, and Z. He, "A novel wpt system based on dual transmitters and dual receivers for high power applications: Analysis, design and implementation," *Energies*, vol. 10, no. 2, 2017. [Online]. Available: https://www.mdpi.com/1996-1073/10/2/174

[14] H. Polat, E. Ayaz, O. Altun, and O. Keysan, "Balancing of common dc-bus parallel connected modular inductive power transfer systems," Sep 2020. [Online]. Available: https://www.techrxiv.org/articles/preprint/Balancing_of_Common_DC-Bus_Parallel_Connected_Modular_Inductive_Power_Transfer_Systems/13013882/2

[15] H. Polat, "Fault tolerant modular inductive power transfer system design using resonator coil," Apr 2021. [Online]. Available: https://www.techrxiv.org/articles/preprint/Fault_Tolerant_Modular_Inductive_Power_Transfer_System_Design_Using_Resonator_Coil/14370617/1

[16] Y. Fang, B. M. H. Pong, and R. S. Y. Hui, "An enhanced multiple harmonics analysis method for wireless power transfer systems," *IEEE Trans. Power Electron.*, vol. 35, no. 2, pp. 1205–1216, 2020.

[17] X. Qu, Y. Jing, J. Lian, S. Wong, and C. K. Tse, "Design for continuous-current-mode operation of inductive-power-transfer converters with load-independent output," *IET Power Electronics*, vol. 12, no. 10, pp. 2458–2465, 2019.

[18] F. Karakaya, O. S. Alemdar, and O. Keysan, "Layout Based Ultra-Fast Short-Circuit Protection Technique for Parallel Connected GaN HEMTs," *IEEE Journal of Emerging and Selected Topics in Power Electronics*, pp. 1–1, 2021.

[19] H. Polat, E. Ayaz, O. Altun, and O. Keysan, "Balancing of common dc-bus parallel connected modular inductive power transfer systems," *IEEE Journal of Emerging and Selected Topics in Power Electronics*, pp. 1–1, 2021.